Orientation dependence and electric-field effect in the relaxor-based ferroelectric crystal $(PbMg_{1/3}Nb_{2/3}O_3)_{0.68}(PbTiO_3)_{0.32}$

Chi-Shun Tu,* C.-L. Tsai, and J.-S. Chen
Department of Physics, Fu Jen University, Taipei 242, Taiwan, Republic of China

V. Hugo Schmidt
Department of Physics, Montana State University, Bozeman, Montana 59717

(Received 4 September 2001; published 1 March 2002)

Dielectric permittivities, polarization–electric-field hysteresis loops, and domain structures have been measured as a function of temperature in relaxor-based ferroelectric single crystals $(PbMg_{1/3}Nb_{2/3}O_3)_{0.68}(PbTiO_3)_{0.32}$ (PMN-32%PT) for $\langle 110\rangle_{cub}$ and $\langle 211\rangle_{cub}$ orientations. Contrary to the pure $PbMg_{1/3}Nb_{2/3}O_3$ (PMN), PMN-32%PT exhibits apparent crystallographic orientation dependences of dielectric permittivities, polarizations, domain structures and phase transitions. With a prior field-cooled treatment, a field-induced state, perhaps of orthorhombic symmetry, is evidenced and coexists with the rhombohedral symmetry in the low-temperature region. This field-induced phase is manifested by an extra dielectric peak observed near 373 K for the $\langle 211\rangle_{cub}$ orientation. A relaxation mechanism which is responsible for the so-called diffuse phase transition crosses a wide temperature region of ~340–400 K and results from fluctuations between rhombohedral and tetragonal states. In order of increasing temperature (without a prior field-cooled treatment), PMN-32%PT undergoes successive phase transformations: rhombohedral phase→coexistence of rhombohedral and tetragonal phases→tetragonal phase→coexistence of tetragonal and cubic phases→cubic phase.

DOI: 10.1103/PhysRevB.65.104113 PACS number(s): 77.80.Bh, 77.80.Dj, 77.22.−d, 77.80.−e

I. INTRODUCTION

Relaxor ferroelectrics generally mean the complex perovskites with an ABO_3-type unit cell and are crystals in which unlike-valence cations belonging to a given site (*A* or *B*) are presented in the correct ratio for charge balance, but are situated randomly on these cation sites.[1–4] These randomly different cation charges give rise to random fields, which tend to make the phase transition ''diffuse'' instead of sharp as in normal ferroelectrics.[3,4] Lead magnesium niobate, $Pb(Mg_{1/3}Nb_{2/3})O_3$ (PMN), is one of the most interesting relaxor ferroelectric (FE) materials. PMN has a disordered complex structure in which the Mg^{2+} and Nb^{5+} cations exhibit only short-range order on the *B* site. Near 280 K the PMN crystal undergoes a diffuse phase transition characterized by a broad frequency-dependent dielectric maximum. PMN has cubic symmetry at room temperature with space group $Pm3m$, whereas a small rhombohedral distortion (pseudocubic) was observed below 200 K.[1,5] Transmission electron microscopy (TEM) investigation has revealed the presence of nanometric scale polar clusters in the relaxor state.[6] The normal FE crystal $PbTiO_3$ (PT) has tetragonal symmetry with space group $P4mm$ at room temperature and has a normal FE phase transition taking place at $T_c = 760$ K with long-range FE order occurring below T_c.[7]

The relaxor-based FE crystals $(PbMg_{1/3}Nb_{2/3}O_3)_{1-x}(PbTiO_3)_x$ (PMN-xPT) naturally has a morphotropic phase boundary (MPB) in the range of ~28–36 mol % of PT.[8] In other words, as temperature decreases, the PMN-xPT crystals ($0.28 \leqslant x \leqslant 0.36$) have successive phase transformations: cubic paraelectric (PE) phase→tetragonal FE phase→rhombohedral FE phase. However, these phase transformations do not exhibit normal FE phase transitions in which clear transition temperatures are defined. In relaxor-based ferroelectrics, the symmetry of the low temperature is broken by quenched disorder. Rather than undergoing a normal phase transformation into the low-temperature state, the system freezes into a state with polar clusters of the low-temperature state embedded within the average symmetry of the high-temperature state. TEM results of MPB compositions of PMN-PT ceramics showed tweedlike structures rather than normal micron-sized domains.[9] These tweedlike structures were oriented along the $\langle 110\rangle$ direction. Domains of $\sim 10^3$ Å in length and $\sim 10^2$ Å in width were reported.[9]

It is well known that in relaxor ferroelectrics the sensitive lattice symmetry is easily affected by external perturbations. Contrary to normal ferroelectrics, an external electric field can enhance phase transition.[10,11] Paik *et al.* showed that a field of 20 kV/cm in the $\langle 001\rangle$-oriented $(PbZn_{1/3}Nb_{2/3}O_3)_{0.92}$-$(PbTiO_3)_{0.08}$ (PZN-8%PT) destroys the rhombohedral state and induces a single tetragonal domain.[10] By *in situ* x-ray diffraction, Durbin *et al.* confirmed that the field-induced crystallographic change occurs at $E \sim 10$ kV/cm from rhombohedral to tetragonal states.[11] It was proposed that under field ($E < 10$ kV/cm) the sample can no longer be perfectly rhombohedral, but that instead it is almost certainly monoclinic.[11] From the electric-field-dependent polarization result, a metastable intermediate orthorhombic FE phase (between rhombohedral and tetragonal states) was proposed to exist in the oriented PZN-8%PT crystal.[12] The unit cell of this intermediate orthorhombic phase is double that of the simple unit cell. This simple unit cell has monoclinic symmetry having the same point group

as that recently suggested by Cross for PZN-PT crystals.[13] In brief, with increasing electric-field strength, PZN-8%PT undergoes successive phase transitions: rhombohedral →orthorhombic→tetragonal. Furthermore, a phenomenological model for MPB compositions of PZT demonstrated that an orthorhombic FE phase is possible as a metastable state between the tetragonal and rhombohedral states.[14] Such an intermediate orthorhombic phase could be enhanced and stabilized under an external electric field. By optical microscopy, with field applied along ⟨001⟩, Belegundu *et al.* confirmed that tetragonal and rhombohedral domains coexist in PZN-8%PT at room temperature and even down to −100 °C.[15] In addition, it has been found that relaxor-based ferroelectrics exhibit large disparity in spatial microheterogeneity and transition temperature.[16,17] Such a fluctuation is believed to result from a quenched unequal occupation of the *B* site by the competitive ions Mg^{2+}, Nb^{5+}, and Ti^{4+}.

Single crystals of PMN-*x*PT have been reported to exhibit much larger piezoelectric constants and electromechanical coupling factors compared with those in the $PbZrO_3$-$PbTiO_3$ (PZT) family of ceramics.[18–20] Such high piezoelectric performance, which converts mechanical and electric energies, is crucial in medical imaging, telecommunication, and ultrasonic devices and may revolutionize these applications.[21] Many works have been undertaken on the growth and characterization of relaxor-based ferroelectrics.[22–30] However, limited attention has been paid to phase coexistence at the MPB.[24,28] The physical mechanism and temperature ranges of the MPB between two different phases (cubic↔tetragonal and tetragonal↔rhombohedral) still remain unclear. An understanding of the mechanism of the electrically induced phase transformation in these crystals has not yet developed. It is believed that the field-induced transformation, phase coexistence, and crystallographical orientation play important roles in the high electromechanical coupling effect. Therefore we carried out temperature-dependent measurements of dielectric permittivity, polarization–electric-field (PEF) hysteresis loop and domain structure on PMN-32%PT for $\langle 110\rangle_{cub}$ and $\langle 211\rangle_{cub}$ oriented crystals.

II. EXPERIMENTAL PROCEDURE

The lead magnesium niobate-lead titanate single crystal PMN-32%PT was grown using a modified Bridgman method.[22] Samples were cut perpendicular to either the $\langle 110\rangle_{cub}$ or $\langle 211\rangle_{cub}$ directions. Here, direction "$\langle\ \rangle_{cub}$" refers to the pseudocubic axes. Physical analysis by the JEOL6100 electron microscope was used to determine concentrations of local *B*-site ions Mg^{2+}, Nb^{5+}, and Ti^{4+}. In the PMN-32%PT platelets that we measured, the Ti^{4+} concentration of each sample varies by about ±2% from its nominal or average composition. The average Ti^{4+} concentration of the $\langle 211\rangle_{cub}$ oriented sample is slight larger (about 0.3%) than the value of the $\langle 110\rangle_{cub}$ oriented sample. Since the MPB is sensitive to the Ti^{4+} content, a slight spatial heterogeneity will result in difference of structural transformation temperatures at the MPB.[8] For measurements of dielectric permittivity and PEF hysteresis loop, sample surfaces were coated with silver paste electrodes. The applied electric fields were along either the $\langle 110\rangle_{cub}$ or $\langle 211\rangle_{cub}$ directions. The average thickness of samples for PEF hysteresis loop experiment is about 0.15 mm. A variable-frequency Wayne-Kerr Precision Analyzer PMA3260A with four-lead connections was used to obtain capacitance and resistance. The heating/cooling rate for dielectric measurement was 1.5 K/min. For the field-cooled–zero-field-heated (FC-ZFH) dielectric measurement, the PMN-32%PT samples were first cooled from 470 K (cubic state) to the rhombohedral phase (≤200 K) with a dc bias field of $E=6$ kV/cm along either the $\langle 110\rangle_{cub}$ or $\langle 211\rangle_{cub}$ directions. Then the dielectric permittivity was measured upon heating without a bias field, i.e., ZFH. The PEF hysteresis loop was measured by using a Sawyer-Tower circuit in which the PEF loop was obtained within 2–4 cycles of electric field at measuring frequency 47 Hz. A Janis CCS-450 closed cycle refrigerator was used with a Lakeshore 340 temperature controller.

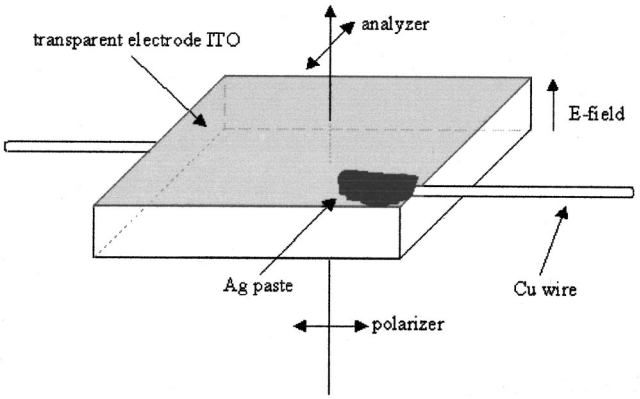

FIG. 1. The experimental configuration for observation of domain structures under the polarized microscope.

The domain structures were studied by using a Nikon E600POL polarized microscope. Transparent conductive ITO (indium tin oxide) films were deposited on sample surfaces by using RF sputtering deposition. Domain structures were observed between a crossed polarizer-analyzer pair along either the $\langle 110\rangle_{cub}$ or $\langle 211\rangle_{cub}$ directions. The experimental configuration for observation of domain structure is illustrated in Fig. 1. For the FC-ZFH domain structures, samples were first cooled from 470 K (cubic state) to 283 K with a dc bias field of $E=7.5$ kV/cm along either the $\langle 110\rangle_{cub}$ or $\langle 211\rangle_{cub}$ directions. Then, domain structures were measured upon heating without a bias field. In order to minimize superposition of domains, the thickness of samples is less than 70 μm. A Linkam THMS600 heating/cooling stage mounted on the microscope was used for studying domain structures as a function of temperature. In the tetragonal phase, spontaneous deformations appear along six equivalent ⟨001⟩ directions and the optical axis (OA) oriented parallels to the ⟨001⟩ polar direction. Adjacent domains of the tetragonal state can be polarized at 90° to each other and form striplike domain walls.[31] Due to strain birefringence and total reflection at the boundary, the 90° domain wall is usually visible in the polarized light. In the rhombohedral phase, the OA is parallel to the ⟨111⟩ polar direction.

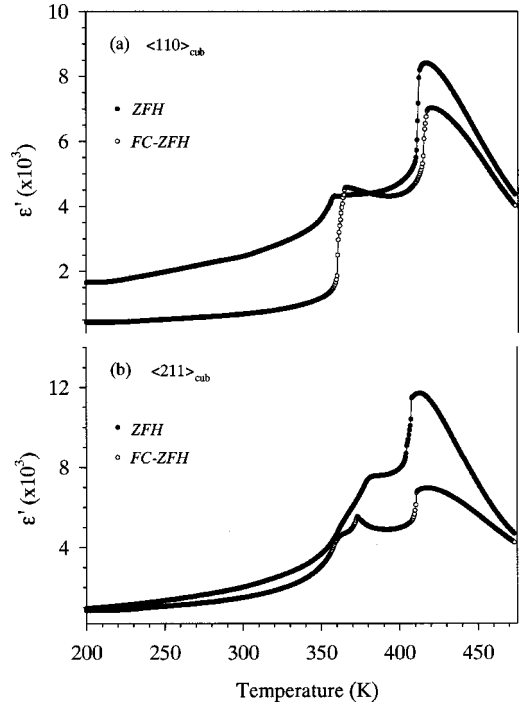

FIG. 2. Temperature dependences of ε' (ZFH) and ε' (FC-ZFH) for (a) $\langle 110\rangle_{\mathrm{cub}}$ and (b) $\langle 211\rangle_{\mathrm{cub}}$ orientations. The dielectric data are taken at $f=10$ kHz upon heating.

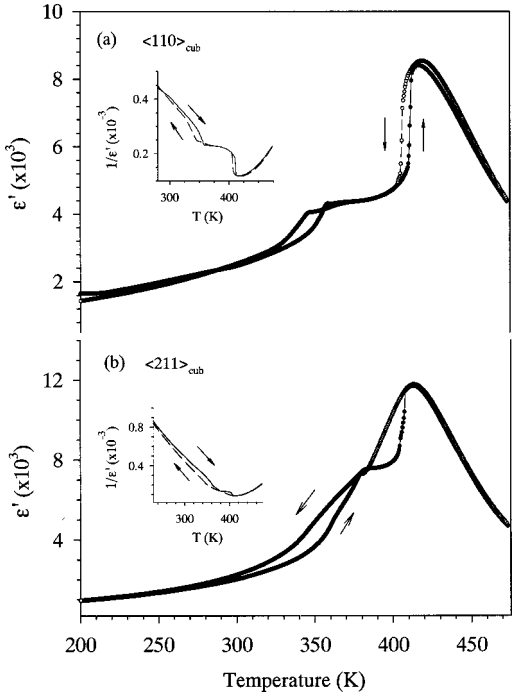

FIG. 3. Thermal hysteresis behaviors of ε' (ZFH) for (a) $\langle 110\rangle_{\mathrm{cub}}$ and (b) $\langle 211\rangle_{\mathrm{cub}}$ orientations taken at $f=10$ kHz. The insets are the reciprocal of ε' (ZFH).

III. RESULTS AND DISCUSSION

Figures 2(a) and (b) show the temperature dependences of the real part ε' of the dielectric permittivity obtained from ZFH and FC-ZFH for $\langle 110\rangle_{\mathrm{cub}}$ and $\langle 211\rangle_{\mathrm{cub}}$ oriented PMN-32%PT crystals, respectively. Due to slight difference in PT content (spatial heterogeneity), $\langle 110\rangle_{\mathrm{cub}}$ and $\langle 211\rangle_{\mathrm{cub}}$ orientations show about 4 K difference in the temperature T_m which corresponds to the maximum of ε' (ZFH). Compared with the ZFH, T_m of the FC-ZFH run was shifted up, respectively, ~3 and ~4 K for $\langle 110\rangle_{\mathrm{cub}}$ and $\langle 211\rangle_{\mathrm{cub}}$ orientations. ε' (ZFH) exhibits a broad plunge accompanied by a frequency dispersion near 360 and 380 K, respectively for $\langle 110\rangle_{\mathrm{cub}}$ and $\langle 211\rangle_{\mathrm{cub}}$ orientations. In particular, ε' (FC-ZFH) of $\langle 110\rangle_{\mathrm{cub}}$ and $\langle 211\rangle_{\mathrm{cub}}$ orientations exhibit a sharp steplike jump near 360 K and an extra peak at 373 K (which superimposes on the broad background of dielectric permittivity), respectively. The temperatures of these anomalies (but not their amplitudes) are independent of frequency. In addition, near 420 K the broad permittivity peak ε'_m (FC-ZFH) of the $\langle 110\rangle_{\mathrm{cub}}$ orientation has magnitude ~7000, about 17% lower than the value of ε'_m (ZFH) ~8400, due to the FC process that reduces domain wall contributions to the dielectric permittivity. For the $\langle 211\rangle_{\mathrm{cub}}$ orientation, the permittivity peak ε'_n (FC-ZFH) near 418 K has magnitude ~7000, about 42% lower than the value of ε'_m (ZFH) ~12 000.

Figure 3 shows two clear thermal hystereses of ε' in the regions of ~280–360 and ~400–415 K. The insets are the reciprocal of ε' in which a typical first-order-like FE phase transition appears near 415 K. We call these first-order transitions (near 360 and 415 K) for two reasons. First, the thermal hysteresis shows that the system is metastable in this temperature region. Metastability can occur for first-but not second-order transitions.[32] Second, the point groups of the tetragonal and rhombohedral symmetries do not have a group-subgroup relation, so a transition between these two symmetries must be of first order.

PEF hysteresis loops are shown in Figs. 4(a) and (b). Spontaneous polarizations (P_s), measured at room temperature, are about 38.7 and 45.4 μC/cm^2 for $\langle 110\rangle_{\mathrm{cub}}$ and $\langle 211\rangle_{\mathrm{cub}}$ orientations, respectively. At room temperature, both $\langle 110\rangle_{\mathrm{cub}}$ and $\langle 211\rangle_{\mathrm{cub}}$ orientations have similar amplitude of coercive field ~5 kV/cm. Coercive fields for different PT contents, measured at room temperature, vary from 3.4 kV/cm (for PMN-24%PT) to 8.0 kV/cm (for PMN-34%PT).[17] However, the coercive field (E_c) of pure $PbTiO_3$ is ~6.8 kV/cm.[33] We cannot explain this E_c dependence, because coercive field is strongly dependent on the rise rate (measuring frequency) of applied field and sample thickness. The thickness dependence of E_c was originally found in $BaTiO_3$ and is attributed to the existence of a space-charge layer.[31]

We now discuss the orientation dependence of P_s. According to the MPB location,[8] near room temperature PMN-32%PT consists of rhombohedral clusters. The fraction of spontaneous polarization along $\langle 110\rangle$ for $\langle 111\rangle$ oriented rhombohedral states must be $\sqrt{2/3}$ [i.e., $\cos(\theta)=(111)\cdot(110)/\sqrt{3}\cdot\sqrt{2}$]. Similarly, the fraction of spontaneous polarization along $\langle 211\rangle$ for $\langle 111\rangle$ oriented rhombohedral states must be $4/3\sqrt{2}$. In other words, the ratio of spontaneous polarization components along $\langle 110\rangle$ and $\langle 211\rangle$ oriented rhombohedral states is $\sqrt{3/2}\approx 0.87$, which is quite consistent with the ratio of measured spontaneous polarizations (obtained at

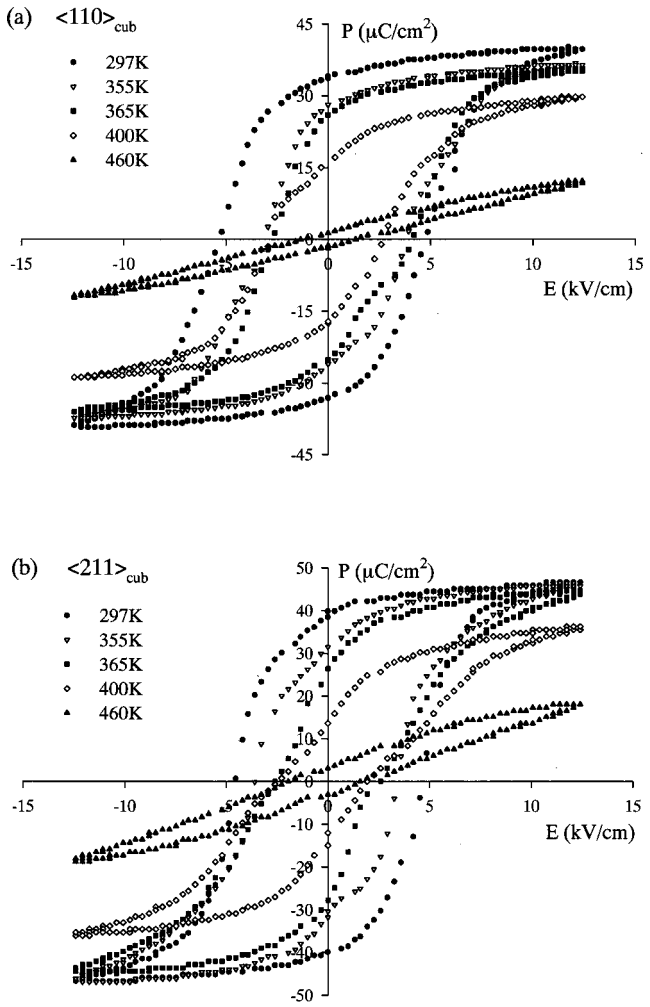

FIG. 4. PEF hysteresis loops of (a) $\langle 110\rangle_{\mathrm{cub}}$ and (b) $\langle 211\rangle_{\mathrm{cub}}$ orientations obtained upon heating.

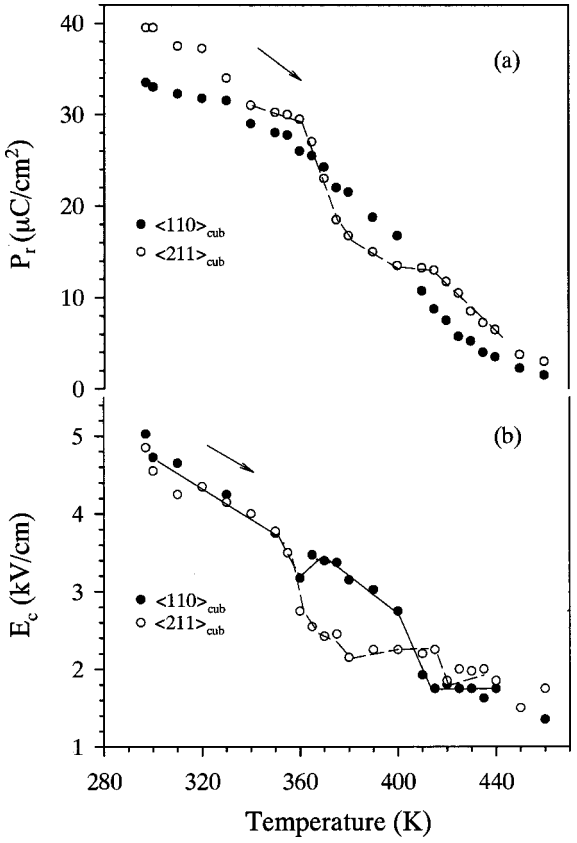

FIG. 5. Temperature dependences of (a) remanent polarization (P_r) and (b) coercive field (E_c) for $\langle 110\rangle_{\mathrm{cub}}$ and $\langle 211\rangle_{\mathrm{cub}}$ orientations upon heating. The dashed and dotted lines are guides for the eye.

room temperature), i.e., $(38.7)/(45.4)\approx 0.85$ (see Fig. 4). Such a crystalline anisotropy of dielectric properties indicates that PMN-32%PT crystal has stronger crystalline distortion than the pure PMN whose average symmetry is cubic near room temperature.[1,5] Temperature-dependent behaviors of remanent polarization (P_r) and E_c are plotted in Fig. 5. Instead of a gradual evolution as seen in PMN,[34] two successive steplike anomalies were observed in both P_r and E_c curves near 360 and 415 K for the $\langle 211\rangle_{\mathrm{cub}}$ orientation. For the $\langle 110\rangle_{\mathrm{cub}}$ orientation, the E_c curve also shows two anomalies near 360 and 415 K. The usual distinctions between first- and second-order transitions, such as discontinuity in dP/dT, do not apply for diffuse phase transitions.

Temperature-dependent domain structures of the $\langle 110\rangle_{\mathrm{cub}}$ orientation are shown in Figs. 6(a) and 6(b), respectively, for ZFH and FC-ZFH. The domain pattern with a cross arrow indicated at the upper right corner was observed in the domain configuration in which the domain matrix exhibits maximum optical extinction at $T=283$ K. As shown in Fig. 6(a), at $T=283$ K, domain structures show complex interference patterns and are mostly associated with the rhombohedral phase. These inhomogeneous interference patterns are probably caused by clusters or microdomains with deviation of the extinction direction from normal crystallographic axes. This deviation may result from the internal stresses caused by the lattice mismatching and the superposition of domains. Since pure PMN crystal remains an optically isotropic pseudocubic state down to very low temperature,[35] complex color domain matrix suggests that a long-range FE phase has been triggered by the substitution of 32% Ti^{4+} for the *B*-site complex ions $(Mg_{1/3}Nb_{2/3})^{4+}$. It is believed that the introduction of Ti^{4+} increases the size of local polar domains by strengthening the off-center displacement and enhances the interactions between polar microdomains, leading to a macroscopic symmetry breaking of the pseudocubic state in small portions of the crystal.

With increasing temperature, striplike 90° domain walls begin to appear near 357 K [see Fig. 6(a)]. It indicates that the tetragonal phase begins to develop near 357 K. This phenomenon implies a slow-moving structural transformation and is consistent with the dielectric result ε' (ZFH) which shows a gradual plunge accompanied by a frequency dispersion near 360 K. As another evidence of a phase transformation from rhombohedral to tetragonal states, the domain matrix at 381 K exhibits maximum optical extinction with rotation angle 35° from the domain configuration given at 283 K. As illustrated in Fig. 7, when observing the $\langle 110\rangle$ oriented sample between a crossed polarizer-analyzer pair along the $\langle 110\rangle$ direction, the angle difference of optical ex-

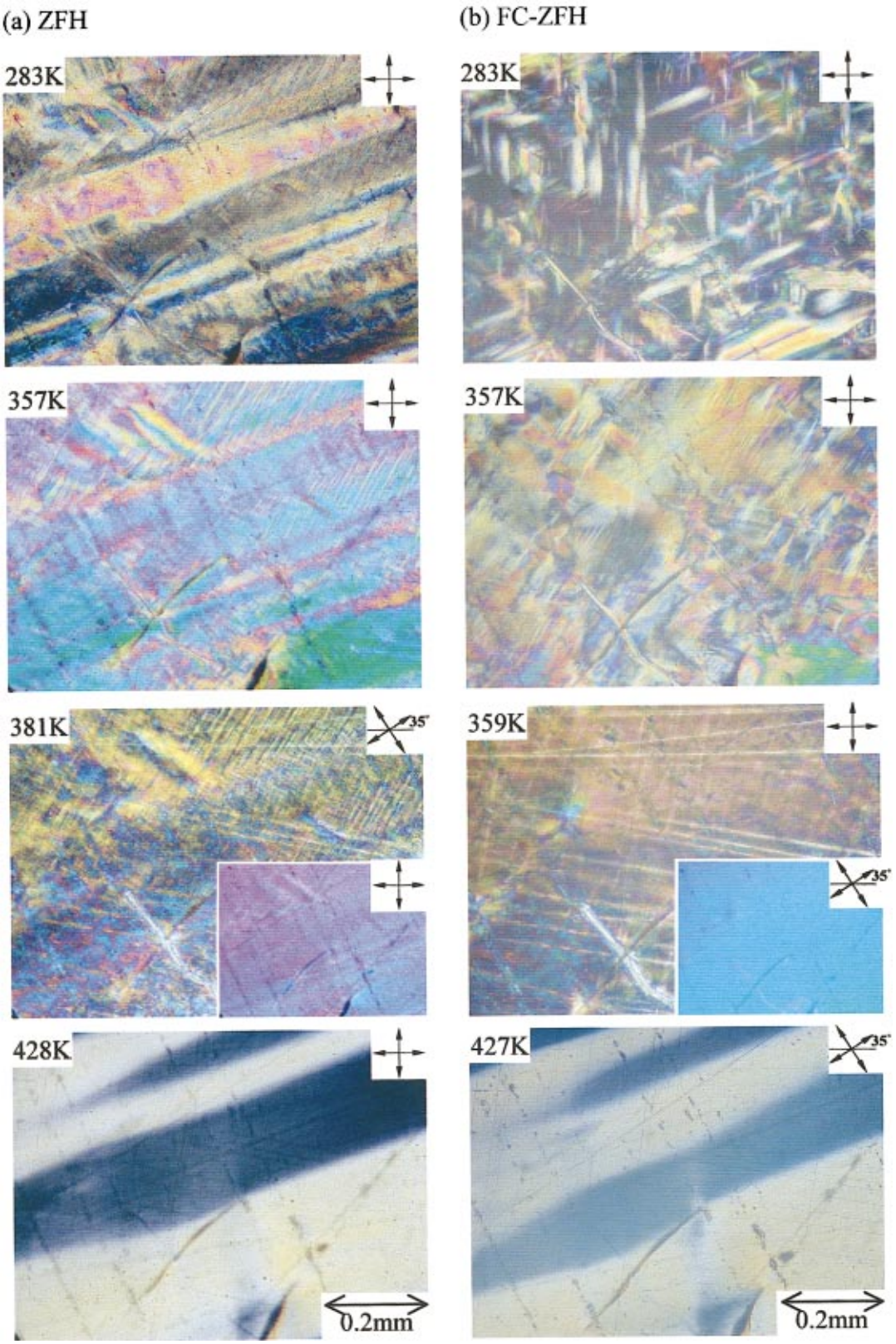

FIG. 6. (Color) Successive domain structures observed along the $\langle 110 \rangle_{cub}$ direction for (a) ZFH and (b) FC-ZFH upon heating.

tinction directions between rhombohedral and tetragonal states is about 35° (or 55°). It confirms that the structure symmetry at 283 K is rhombohedral. Upon further heating, the isotropic cubic phase corresponding to striplike dark regions illustrated at 428 K of Fig. 6(a) begins to develop near 428 K. Then, the crystal turns into the cubic state completely near 430 K which is higher than the temperature T_m of ε' (ZFH). On the whole, PMN-32%PT possesses a coexistence

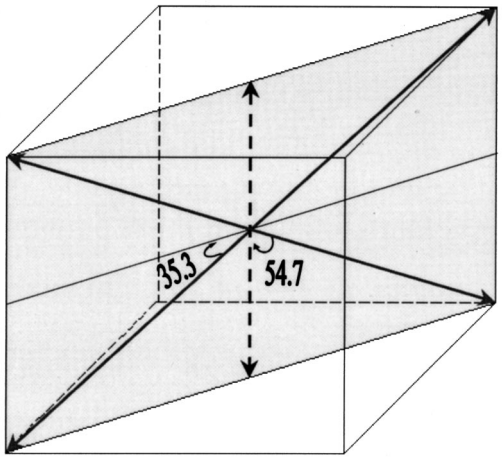

FIG. 7. Schematics of domain configuration for the ⟨110⟩ orientation. Solid and dashed arrow lines indicate respectively projections of polar directions of rhombohedral and tetragonal states on the [110] face.

phase of rhombohedral and tetragonal states from about 360 K, and reaches the tetragonal state entirely near 380 K. Before turning into the cubic phase, the ⟨110⟩ oriented crystal exhibits another coexistence phase of tetragonal and cubic states in a narrow temperature range of ~428–430 K.

Domain structures obtained from the FC-ZFH, as given in Fig. 6(b) at 283 K, show mixture of dark domain regions and complex color domains. This phenomenon implies that a field-induced phase (dark domain regions) coexists with the rhombohedral state in the low-temperature domain matrix. This field-induced phase possibly corresponds to the orthorhombic state as proposed recently by Viehland for the PZN-8%PT crystal.[12] On the other hand, a field-induced tetragonal phase was observed in the PZN-8%PT system under a stronger electric field.[10,11] In the tetragonal state, the direction of optical extinction is parallel to the ⟨001⟩ polar direction. Thus this field-induced phase may include both orthorhombic and tetragonal symmetries. Upon heating, as shown at $T=357$ K, complex color regions gradually increases in the domain matrix. Such a phenomenon indicates that the field-induced phase was partially perturbed by thermal energy with increasing temperature, and results in partial conversion of domain regions converting into the rhombohedral phase characterized with a complex color domain matrix. In addition, striplike 90° domain walls were also seen in the domain matrix at $T=357$ K. Near 359 K, striplike 90° domain walls disappear. The inset at $T=359$ K illustrates a uniform domain matrix observed from the domain configuration with rotation angle 35°. This phenomenon indicates that the crystal turns into the tetragonal state entirely near 359 K. It is consistent with the dielectric result ε' (FC-ZFH) which shows a sharp steplike temperature-dependent behavior near 360 K, implying a normal phase transition. Upon further heating, the isotropic cubic phase begins to enter near 427 K. Finally, the crystal turns into the cubic state completely near 430 K.

In the ZFH case [Fig. 8(a)] of the $\langle 211\rangle_{cub}$ orientation, domain structures at 283 K exhibit complex interference patterns that are mostly associated with the rhombohedral state. With increasing temperature, the domain matrix becomes brighter and striplike 90° domain walls begin to appear near 360 K. This phenomenon indicates that the tetragonal phase begins to develop near 360 K in the crystal. It is consistent with the dielectric result ε' (ZFH) which shows a gradual plunge in the region of ~360–380 K. As another evidence of phase transformation (rhombohedral→tetragonal), the domain matrix (see the inset at 380 K) exhibits maximum optical extinction with rotation angle about 31° from the domain configuration given at 283 K. When observing the ⟨211⟩ oriented sample between a crossed polarizer-analyzer pair along the ⟨211⟩ direction, the angle difference of optical extinction directions between rhombohedral and tetragonal states is about 39°. This change of optical extinction directions between 283 and 380 K implies a phase transformation. The cause of the angle deviation between 31° (measured value) and 39° (calculated value) is not clear. It may result from the superposition of domains and the orientation deviation due to polishing the sample. However, compared with the $\langle 110\rangle_{cub}$ orientation, the optical extinction configuration of the $\langle 211\rangle_{cub}$ orientation is more complicated. Upon further heating, the cubic state begins to develop near 417 K and then the crystal turns into the cubic state completely near 420 K.

FC-ZFH domain structures of the $\langle 211\rangle_{cub}$ orientation, as given at 283 K in Fig. 8(b), show a mixture of dark domain regions and complex color domains. It indicates that the field-induced phase (dark regions) coexists with the rhombohedral state in the low-temperature region. With increasing temperature, as shown at $T=360$ K, dark regions gradually reduce and more color domain regions appear. This phenomenon evidences that the field-induced phase was partially perturbed by thermal energy with increasing temperature, and results in partial conversion of domain regions converting into the rhombohedral phase. Near 373 K, the crystal suddenly transforms into a uniform domain matrix which corresponds to a long-range tetragonal. As temperature increases, the cubic phase begins to establish near 419 K and then the crystal turns into the cubic state completely near 420 K.

Probably the most convincing evidence for the field-induced, possibly orthorhombic, phase is the extra peak in the zero-field-heated dielectric permittivity ε' (FC-ZFH) shown at 373 K after field cooling in a dc bias field [see Fig. 2(b)]. The ε' (FC-ZFH) exhibits successively a gradual plunge and an extra peak at 360 and 373 K. These continuous temperature-dependent anomalies possibly imply sequential phase transformatios: rhombohedral →orthorhombic→tetragonal. Similar phase transformations were seen in the $BaTiO_3$ system in which a stable orthorhombic FE phase was observed between the FE rhombohedral and FE tetragonal phases.[36] During the FC process, the external electric-field bias along the ⟨211⟩ direction could cause polar displacement to deviate from the ⟨111⟩ direction in the unit cell of the rhombohedral phase, resulting in the lack of threefold symmetry with only mirror symmetry on the {011} plane. An orthorhombic (*O*) phase occurring near the rhombohedral-tetragonal (*R*-*T*) morphotropic phase

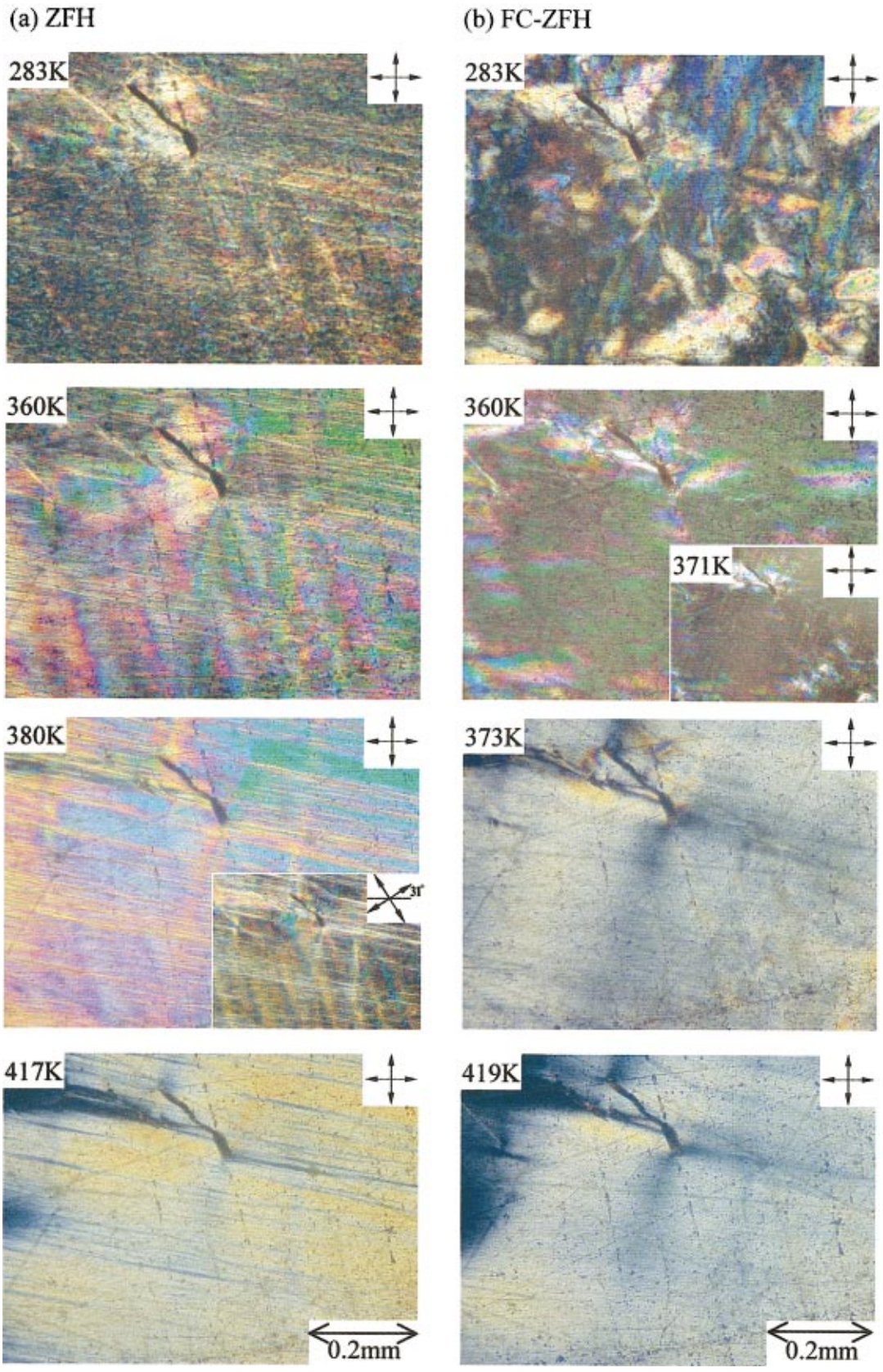

FIG. 8. (Color) Successive domain structures of (a) ZFH and (b) FC-ZFH for the $\langle 211 \rangle_{cub}$ orientation.

boundary in this crystal could occur for two reasons. First, this phase could be thermodynamically stable even in the absence of stress energy considerations. Second, the phase may only be metastable in the absence of stress energy considerations. That is, at the morphotropic phase boundary, the *R* and *T* phases would have the same free energy, but the *O* phase would have higher free energy. We now consider a special case that illustrates how an *O* phase domain could become stable because it reduces the wall energy between *R* and *T* ferroelectric domains.

We consider a *T* domain with primitive cell vectors [1,0,0], [0,1,0], [0,0,1+Δ] in units of the cubic cell length *a*. This cell has polarization along [001]. We then consider an adjacent *R* domain with primitive cell vectors [1 $+\delta/3,\delta/3,\delta/3$] and its two permutations, that has polarization along [111]. For a boundary between domains that are adjacent along the *x* axis, we are interested in the scalar product of the normalized perpendiculars to the *yz* faces, because this product is the cosine of the mismatch angle. This product is $[1,0,0]\cdot[1-\delta^2/9,-\delta/3,-\delta/3]=1-\delta^2/9$. Since $\cos\theta_{RT}\cong 1-{\theta_{RT}}^2/2$, $\theta_{RT}\cong\sqrt{2}\,\delta/3$ is the *R*-*T* mismatch angle, so the parameter U_{RT} proportional to the wall energy, subject to the above approximations, is $U_{RT}=2\,\delta^2/9$.

There are three orthorhombic (*O*) cell types with polarization intermediate between those of the above *R* and *T* cells. We choose the one with polarization along [101] for this illustration. Its unit cell has double volume compared to the *R* and *T* cells, so we must use its pseudomonoclinic primitive cell with translation vectors $[1+\alpha/2,0,\alpha/2]$, [0,1,0], $[\alpha/2,0,1+\alpha/2]$ for calculating the mismatch angles. The normalized perpendicular to its *yz* face is $[1-\alpha^2/8,0,-\alpha/2]$. Its scalar products with its neighboring *T* and *R* domain perpendiculars are $1-\alpha^2/8$ and $1-\alpha^2/8-\delta^2/9+\alpha\delta/6$, respectively. The corresponding angles are $\theta_{TO}=\alpha/2$ and $\theta_{RO}=(\alpha^2/4-\alpha\delta/3+2^2/9)^{1/2}$, and the corresponding energy parameters are $U_{TO}=\alpha^2/4$ and $U_{RO}=\alpha^2/4-\alpha\delta/3+2\,\delta^2/9$. The overall wall energy parameter is the sum of these two parameters. If we assume that there is no energy penalty for the orthorhombic distortion parameter α to adjust itself so as to minimize this sum, then $\alpha_{\min}=\delta/3$. Substituting this value into the energy sum yields $(U_{TO}+U_{RO})_{\min}=\delta^2/6$. This is only $\frac{3}{4}$ of the energy parameter for no intervening *O* domain. The conclusion of this illustration is that it is plausible that an otherwise metastable orthorhombic phase can be stabilized if it acts as a buffer between tetragonal and rhombohedral phases. Because the *R* and *T* phases can coexist over a wide temperature range, there is opportunity for small orthorhombic domains to exist over such a temperature range.

The above illustration is not a complete calculation because, while it assumes stress energy proportional to domain mismatch angle, it does not take into account how far the stress field penetrates into each domain. Such information, together with the free energy excess of the *O* phase relative to the *R* and *T* free energy, is necessary in order to place lower and upper limits on the thickness allowed for stress-stabilized *O* domains. Also, one must use the elastic moduli and primitive cell volumes for each phase in a complete calculation, instead of assuming them the same for each phase as is done in the above illustration.

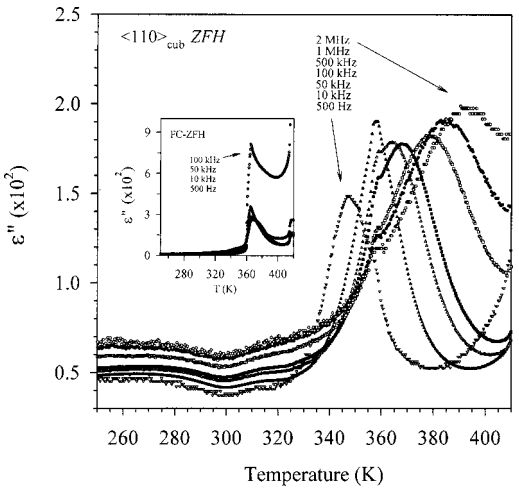

FIG. 9. Temperature and frequency dependences of ε'' (ZFH) obtained for the $\langle 110\rangle_{\rm cub}$ orientation. The inset illustrates the temperature-dependent ε'' (FC-ZFH).

In the low-temperature region, ε' (ZFH) of the $\langle 110\rangle_{\rm cub}$ orientation [Fig. 2(a)] exhibits a gradual change near 360 K. As shown in Fig. 9, ε'' (ZFH) shows an obvious relaxation behavior in the corresponding temperature region. Similar frequency-dependent dielectric anomalies were seen in PZN-PT and other PMN-PT systems.[7,17,24,37,38] As evidenced earlier in the ZFH case, temperature-dependent domain structures reveal that a coexistence phase of rhombohedral and tetragonal states exists in the region of ~360–380 K. Thus the diffuse phase transition near 360 K could be attributed to structural fluctuations between local rhombohedral and tetragonal states.

The temperature- and frequency-dependent composite shapes of ε'' (ZFH) imply that two mechanisms are involved in the region of the diffuse phase transition (~340–400 K). To check this, the experimental results were fitted to two Gaussian functions,

$$\varepsilon''(\mathrm{ZFH})=A\exp\left[\frac{-1}{2}\left(\frac{T-T_{g\mathrm{I}}}{\Delta_{\mathrm{I}}}\right)^2\right]+B\exp\left[\frac{-1}{2}\left(\frac{T-T_{g\mathrm{II}}}{\Delta_{\mathrm{II}}}\right)^2\right], \quad (1)$$

where $T_{g\mathrm{I}}$ and $T_{g\mathrm{II}}$ are temperatures corresponding to peaks of ε'' (ZFH) in the region of ~340–400 K. Figure 10 illustrates fits of two Gaussian functions at three measuring frequencies for the $\langle 110\rangle_{\rm cub}$ orientation. The stronger peak, as indicated by "I," was found to be frequency dependent. This phenomenon indicates that a frequency-dependent relaxation process exists in the region of ~340–400 K. This relaxation mechanism is believed to be responsible for the so-called diffuse transition, and results from fluctuations between rhombohedral and tetragonal states. In addition, peak "II" (which has smaller amplitude) located near 358 K, was found to be frequency independent. With temperature-dependent anomalies of ε' (ZFH) and domain structures near 357 K [Figs. 2(a) and 6(a)], it is reasonable to conclude that the peak II should be associated with the establishment of the long-range FE tetragonal phase.

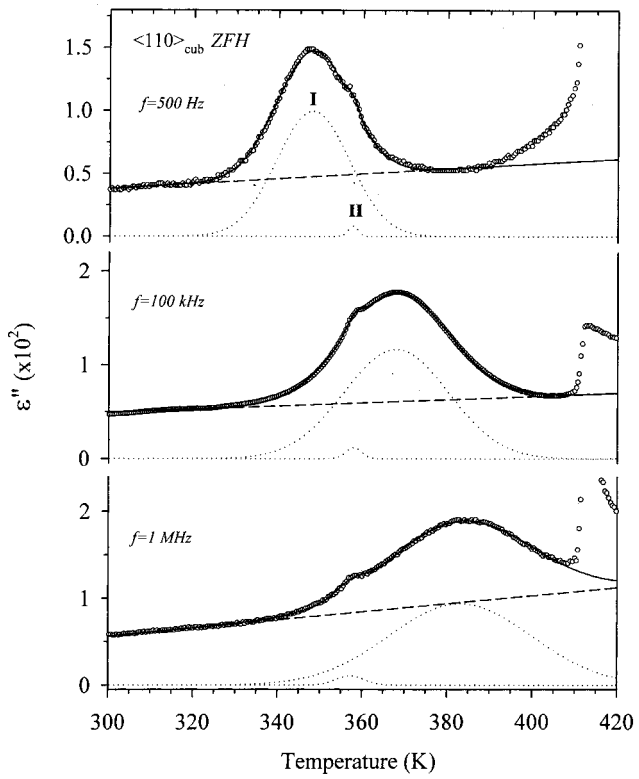

FIG. 10. Illustrations of the best fits in ε'' (ZFH) with two Gaussian functions for the $\langle 110\rangle_{\mathrm{cub}}$ orientation.

As illustrated in the inset of Fig. 9, near 360 K ε'' (FC-ZFH) exhibits a sharp anomaly superimposed on the broad background. The temperature for this anomaly (but not its amplitude) is almost independent of frequency. It implies that the relaxation mechanism which appears in ε'' (ZFH) was greatly reduced after the FC process. In other words, the external field could suppress the diffuse phase transition and enhances occurrence of long-range percolating clusters.

Similar temperature- and frequency-dependent dielectric behaviors, as shown in Figs. 11 and 12, were observed for the $\langle 211\rangle_{\mathrm{cub}}$ oriented crystal. Figure 12 illustrates fits of two Gaussian functions for three measuring frequencies. Peak I was found to be frequency dependent and corresponds to a relaxation process. The peak II located near 380 K, was found to be frequency independent and correlates to long-range percolating clusters. This temperature is consistent with the temperature corresponding to the steplike plunge in ε' (ZFH) and appearance of 90° domain walls which is a character of the tetragonal state.

As shown in Fig. 13, it was found that the relaxation process associated with peak I obeys the exponential Vogel-Fulcher equation that has been used to describe other relaxation process in mixed systems:

$$f = f_o e^{-E_a/K(T_g - T_o)}, \tag{2}$$

where f is the measured frequency, f_o is the attempt frequency, and E_a is the activation energy for orientation of electric dipoles. T_o is the Vogel-Fulcher temperature (static freezing temperature) and T_g is the temperature where ε'' (ZFH) reaches its maximum value. The fitting results of the activation energy, attempt frequency, and Vogel-Fulcher temperature for $\langle 110\rangle_{\mathrm{cub}}$ and $\langle 211\rangle_{\mathrm{cub}}$ orientations are given in Table I. What is the significance of these parameters? First, attempt frequencies are in the usual range for lattice vibration frequency. Second, T_o is the temperature at which, based on an unjustified extrapolation of the Vogel-Fulcher formula beyond the range of the data, all reorientation would cease. Third, E_a is the average of activation potential barriers for various clusters in this disordered system to reorient between

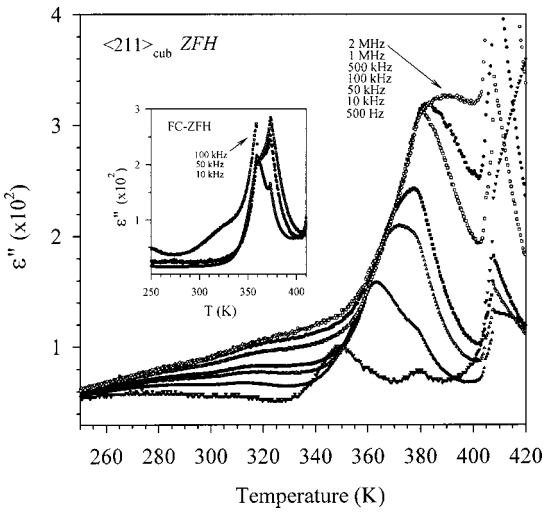

FIG. 11. Temperature and frequency dependence of ε'' (ZFH) obtained for the $\langle 211\rangle_{\mathrm{cub}}$ orientation. The inset illustrates the temperature-dependent ε'' (FC-ZFH).

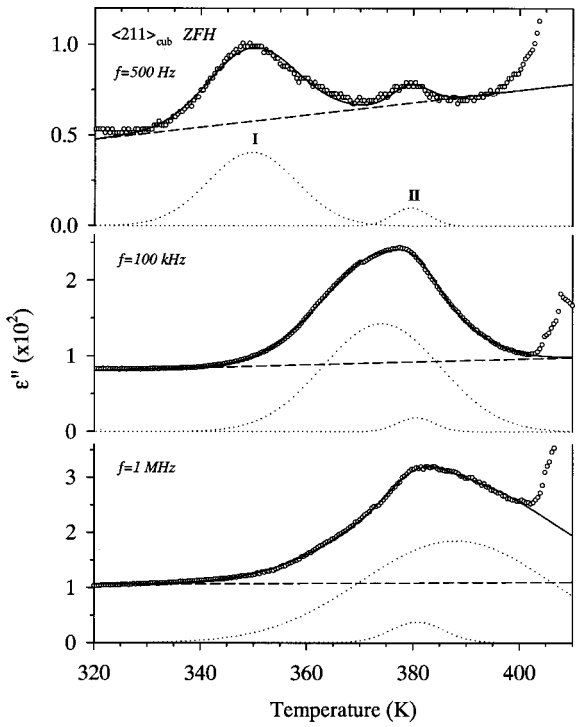

FIG. 12. Illustrations of the best fits in ε'' (ZFH) with two Gaussian functions for the $\langle 211\rangle_{\mathrm{cub}}$ orientation.

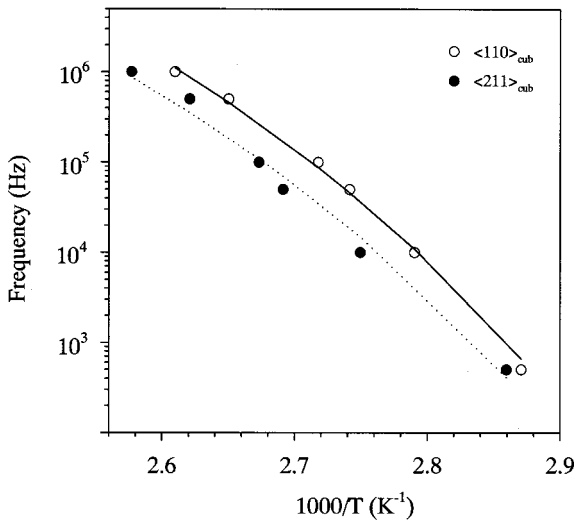

FIG. 13. Frequency vs 1000/T. "T" is the temperature corresponding to the maximum value of ε'' (ZFH) in the region of ~340–400 K. The solid and dotted lines are fits of Eq. (2) with parameters given in Table I.

adjacent variants. As given in Table I, the activation energy and Vogel-Fulcher temperature are the same for $\langle 110\rangle_{cub}$ and $\langle 211\rangle_{cub}$ orientations. Compared with PMN-5%PT and PMN-10%PT ceramics whose activation energies are 0.046 and 0.041 eV, respectively,[39,40] the higher activation energy in PMN-32%PT implies a stronger correlation between polar clusters, which gives rise to a slower process to reach equilibrium in the system. In other words, the relaxation process in the PMN-32%PT takes a longer time and makes it more difficult for the normal phase transition to occur.

IV. CONCLUSIONS

In this report, three important features have been found from $\langle 110\rangle_{cub}$ and $\langle 211\rangle_{cub}$ oriented PMN-32%PT crystals. First, PMN-32%PT exhibits apparent crystallographical orientation dependences of dielectric permittivities, polarizations, domain structures, and phase transitions. Second, with a prior field-cooled process from the cubic state, a field-induced state, perhaps of orthorhombic symmetry, is observed and coexists with the rhombohedral symmetry in the low-temperature region. This partial field-induced effect also enhances a sharp steplike jump and an extra peak in dielectric permittivity appeared near 360 and 373 K for $\langle 110\rangle_{cub}$ and $\langle 211\rangle_{cub}$ orientations, respectively. Third, in the ZFH case, PMN-32%PT undergoes successive phase transformations: rhombohedral phase→coexistence of rhombohedral and tetragonal phases→tetragonal phase→coexistence of tetragonal and cubic phases→cubic phase. The temperature range of coexistence phase between rhombohedral and tetragonal states is much wider than the temperature range of coexistence phase between tetragonal and cubic states. In addition, a relaxation mechanism which is responsible for the so-called diffuse transition crosses a wide-temperature region of ~340–400 K. It was evidenced that an external electric field can suppress this relaxation behavior and enhances long-range percolating polar clusters.

TABLE I. Activation energies (E_a), Vogel-Fulcher temperatures (T_o), and attempt frequencies (f_o) from fits of Eq. (2) for $\langle 110\rangle_{cub}$ and $\langle 211\rangle_{cub}$ orientations.

	E_a (eV)	T_o (K)	f_o (Hz)
$\langle 110\rangle_{cub}$	0.13	279	2.9×10^{12}
$\langle 211\rangle_{cub}$	0.13	279	1.2×10^{12}

ACKNOWLEDGMENTS

The authors would like to express sincere thanks to Mr. Cheng-Chung Lin for depositing ITO (indium tin oxide) transparent electrode. This work was supported by Grant No. NSC90-2112-M-030-001 and DoD EPSCoR Grant No. N00014-99-1-0523.

*Author to whom correspondence should be addressed. Electronic address: phys1008@mails.fju.edu.tw

[1] L. E. Cross, Ferroelectrics **76**, 241 (1987).
[2] D. Viehland, M. Wuttig, and L. E. Cross, Ferroelectrics **120**, 71 (1991).
[3] V. Westphal and W. Kleemann, and M. D. Glinchuk, Phys. Rev. Lett. **68**, 847 (1992).
[4] Z.-G. Ye, Key Eng. Mater. **155–156**, 81 (1998).
[5] L. A. Shebanov, P. Kaspostins, and J. Zvirgzds, Ferroelectrics **56**, 1057 (1984).
[6] C. Randall, D. Barber, and R. Whatmore, J. Microsc. **45**, 275 (1987).
[7] M. L. Mulvihill, S. E. Park, G. Risch, Z. Li, and K. Uchino, Jpn. J. Appl. Phys., Part 1 **35**, 3984 (1996).
[8] T. R. Shrout, Z. P. Chang, N. Kim, and S. Markgraf, Ferroelectr. Lett. Sect. **12**, 63 (1990).
[9] D. Viehland, M. Kim, Z. Xu, and J. Li, Appl. Phys. Lett. **67**, 2471 (1995).
[10] D. S. Paik, S. E. Park, S. Wada, S. F. Liu, and T. R. Shrout, J. Appl. Phys. **85**, 1080 (1999).
[11] M. K. Durbin, E. W. Jacobs, J. C. Hicks, and S.-E. Park, Appl. Phys. Lett. **74**, 2848 (1999).
[12] D. Viehland, J. Appl. Phys. **88**, 4794 (2000).
[13] L. E. Cross, *Workshop on Piezoelectric Crystals*, Arlington, VA, 2000.
[14] A. Amin, M. J. Haun, B. Badger, H. McKinstry, and L. E. Cross, Ferroelectrics **65**, 107 (1985).
[15] U. Belegundu, X. H. Du, and K. Uchino, Ferroelectrics **222**, 67 (1999).
[16] F. M. Jiang and S. Kojima, Appl. Phys. Lett. **77**, 1271 (2000).
[17] C.-S. Tu, C.-L. Tsai, V. H. Schmidt, H. Luo, and Z. Yin, J. Appl. Phys. **89**, 7908 (2001).
[18] S.-E. Park and T. R. Shrout, J. Appl. Phys. **82**, 1804 (1997).
[19] Y. Yamashita, Jpn. J. Appl. Phys., Part 1 **33**, 5328 (1994).
[20] S. W. Choi, T. R. Shrout, S. J. Jang, and A. S. Bhalla, Ferroelectrics **100**, 29 (1989).

[21] R. F. Service, Science **275**, 1878 (1997).
[22] H. Luo, G. Xu, P. Wang, and Z. Yin, Ferroelectrics **231**, 97 (1999).
[23] H. Fu and R. E. Cohen, Nature (London) **403**, 281 (2000).
[24] C.-S. Tu, F.-C. Chao, C.-H. Yeh, C.-L. Tsai, and V. H. Schmidt, Phys. Rev. B **60**, 6348 (1999).
[25] S. Gentil, G. Robert, N. Setter, P. Tissot, and J.-P. Rivera, Jpn. J. Appl. Phys., Part 1 **39**, 2732 (2000).
[26] M. K. Durbin, J. C. Hicks, S.-E. Park, and T. R. Shrout, J. Appl. Phys. **87**, 8159 (2000).
[27] S. Saitoh, T. Kobayashi, K. Harada, S. Shimanuki, and Y. Yamashita, Jpn. J. Appl. Phys., Part 1 **37**, 3053 (1998).
[28] G. Ye and M. Dong, J. Appl. Phys. **87**, 2312 (2000).
[29] H. Luo, G. Xu, H. Xu, P. Wang, and Z. Yin, Jpn. J. Appl. Phys., Part 1 **39**, 5581 (2000).
[30] E. M. Sabolsky, S. Kwon, E. Suvaci, A. R. James, G. L. Messing, and S. Trolier-McKinstry, *Proceedings of the 12th IEEE International Symposium on the Application of Ferroelectrics (ISAF)*, 2001, p. 393.
[31] F. Jona and G. Shirane, *Ferroelectric Crystals* (Dover, New York, 1993).
[32] M. E. Lines and A. M. Glass, *Principles and Applications of Ferroelectrics and Related Materials* (Oxford, London, 1977).
[33] J. P. Remeika and A. M. Glass, Mater. Res. Bull. **5**, 37 (1970).
[34] V. A. Bokov and I. E. Mylnikov, Sov. Phys. Solid State **3**, 613 (1961).
[35] Z.-G. Ye and H. Schmid, Ferroelectrics **145**, 83 (1993).
[36] J. Merz, Phys. Rev. **76**, 1221 (1949).
[37] C.-S. Tu, V. H. Schmidt, H. Luo, and F. C. Chao, Ferroelectr. Lett. Sect. **27**, 49 (2000).
[38] V. H. Schmidt, C.-S. Tu, and B.-C. Cheng, *Proc. of the 12th IEEE International Symposium on the Application of Ferroelectrics (ISAF)*, 2001, p. 283.
[39] H. K. Guo, X. G. Tang, and J. X. Zhang, J. Mater. Sci. Lett. **17**, 1567 (1998).
[40] D. Viehland, S. J. Jang, and L. E. Cross, J. Appl. Phys. **68**, 2916 (1990).